

Modelling of Adsorption of Methane, Nitrogen, Carbon Dioxide, Their Binary Mixtures, and Their Ternary Mixture on Activated Carbons Using Artificial Neural Network

H. Barki, L. Khaouane,* and S. Hanini

This work is licensed under a
Creative Commons Attribution 4.0
International License



Laboratory of Biomaterial and Transport Phenomena (LBMPT), University of Médéa, Algeria

Abstract

This work examines the use of neural networks in modelling the adsorption process of gas mixtures (CO_2 , CH_4 , and N_2) on different activated carbons. Seven feed-forward neural network models, characterized by different structures, were constructed with the aim of predicting the adsorption of gas mixtures. A set of 417, 625, 143, 87, 64, 64, and 40 data points for NN1 to NN7, respectively, were used to test the neural networks. Of the total data, 60 %, 20 %, and 20 % were used, respectively, for training, validation, and testing of the seven models. Results show a good fit between the predicted and experimental values for each model; good correlations were found ($R = 0.99656$ for NN1, $R = 0.99284$ for NN2, $R = 0.99388$ for NN3, $R = 0.99639$ for Q_1 for NN4, $R = 0.99472$ for Q_2 for NN4, $R = 0.99716$ for Q_1 for NN5, $R = 0.99752$ for Q_3 for NN5, $R = 0.99746$ for Q_2 for NN6, $R = 0.99783$ for Q_3 for NN6, $R = 0.9946$ for Q_1 for NN7, $R = 0.99089$ for Q_2 for NN7, and $R = 0.9947$ for Q_3 for NN7). Moreover, the comparison between the predicted results and the classical models (Gibbs model, Generalized dual-site Langmuir model, and Ideal Adsorption Solution Theory) shows that the neural network models gave far better results.

Keywords

Activated carbons, adsorption, gas mixture, modelling, neural network

1 Introduction

Most applications of solids in industry involve porous materials and adsorption processes.¹ Multicomponent adsorption equilibrium is the theoretical basis of designing a separation process based on adsorption.^{2,3} It is a process whereby two or more components of a fluid (gas or liquid) stream are separated through contact with a solid surface. The quantity of the component that is able to bind to the surface of the adsorbent will depend on the temperature and the composition (partial pressure or concentration), as well as various physical and chemical properties of the adsorbate-adsorbent pair. A measurement of the amount adsorbed over a range of compositions at a fixed temperature is known as an adsorption isotherm.⁴

Adsorption represents an important process for separation and purification processes within many domains of the chemical industry.^{5,6} Adsorption has been widely used in environmental chemistry because of its relatively low cost, simplicity of design, and capacity for adsorbing a board range of pollutants at low concentration.^{7,8} Gas adsorption is of particular interest especially because it is involved in numerous processes linked to environmental protection.⁹ Activated carbon is the most commonly used and most effective modified adsorbent support because of its high specific surface area,¹⁰ low acid/base reactivity, thermodynamically stable nature, and porous structure with high controllability,^{11,12} compared to other adsorbents such as zeolite and silica.^{13–15} Moreover, it can be produced in large quantities inexpensively.^{11,16}

An accurate assessment of the equilibrium and kinetics of adsorption is very important for the design and operation of adsorption-based processes.¹ A number of models to predict the adsorption equilibria have been proposed by many investigators¹⁷ such as Langmuir model,¹⁸ Freundlich model,¹⁹ Sips model,²⁰ and Toth model.²¹ These models are used to predict only the adsorption of the pure component system. Therefore, mathematical models have been developed to predict multicomponent adsorption equilibrium based on the adsorption information of each component.^{22–25} These models are roughly classified into five groups: (1) extended Langmuir (EL) model; (2) ideal adsorption solution theory;²⁶ (3) vacancy solution theory;^{27–29} (4) statistical thermodynamic model;^{30,31} (5) Polanyi potential theory;³² and other classical models. Each model had some degree of success, and was limited to a few specific systems.² To avoid these limitations, the application of assumption-free models is proposed. *M. Hasanzadeh et al.*³³ propose a new simplified local density model for adsorption of pure gases and binary mixtures on activated carbon. It was shown that the new SLD model can correlate adsorption data for different pressures and temperatures with minimum error.³³ *Arpita Ghosh et al.*³⁴ propose the modelling of biosorption of Cu (II) by alkali-modified spent tea leaves using response surface methodology (RSM) and artificial neural network (ANN).³⁴ ANN is one of the data-based non-traditional tools for modelling the adsorption process. ANN modelling has been successfully used for the adsorption process in the past decade.³⁵ Feedforward neural networks have been successfully used in many applications related to adsorption. It has been used to simulate the dynamics of an adsorption column for wastewater treatment of water containing toxic chemicals.³⁶ *Kumar et al.*³⁷

* Corresponding author: Latifa Khaouane, Doctor
Email: latifa_khaouane@yahoo.fr

used a three-layer feedforward artificial neural network to model the equilibrium data of hydrogen onto activated carbons,³⁷ the properties of the activated carbons and the experimental conditions were used as inputs to predict the corresponding hydrogen uptake at equilibrium conditions.⁴ *Cojocar et al.*³⁸ constructed a feedforward artificial neural network to predict the removal efficiency of an oil slick from the water surface by peat sorbent. Adsorbent dose, drainage time, and the initial thickness of the oil slick were used as inputs of the neural network to predict the removal efficiency as output. The mean square error (MSE) value of the network was found to be $4.979 \cdot 10^{-4}$.³⁸ *Aghav et al.*³⁹ used a three-layer feedforward neural network with back propagation algorithm for estimation of removal efficiencies of phenol and resorcinol, in bi-solute water, by some carbonaceous adsorbents.³⁹ The input parameters used for training the neural network include the amount of adsorbent, initial concentrations of phenol and resorcinol, contact time, and pH. Removal efficiencies of phenol and resorcinol were considered as outputs of the neural network.³⁵ With the artificial neural network, *M. Molashahi et al.* simulated the adsorption of methane on activated carbon. The input parameters of the applied ANN model were pressure, temperature, and surface area of the adsorbent, the performance of the ANN model was measured using mean square error as $3.053916 \cdot 10^{-3}$ and a correlation coefficient of 0.998.⁴⁰

This study applied ANN models to predict the adsorption amount of pure gases (CO_2 , CH_4 , and N_2), their binary mixtures, and their ternary mixture, onto different activated carbons. For this purpose, a database of 1440 set was selected from different works in literature. Feedforward ANN models with BFGS algorithm was applied to predict the adsorption amount. The predicted results found from the optimized ANN models were compared with the experimental data in order to find models that adequately predict equilibrium data.

2 Experimental

2.1 Theory

Artificial neural networks are analytical models capable of identifying logical patterns in sets of data that were developed to mathematically mimic the characteristics of biological neural networks.⁴¹ Artificial Neural Network (ANN) models were designed in the second half of the 20th century by mathematical simulation of the procedures on which the human nervous system works.^{11,42,43} It consists of a number of interconnected simple processing units called artificial neurons. One of the most popular neural network paradigms applied to the modelling of a wide range of nonlinear systems, especially chemical and biological engineering processes, is the feedforward neural network (FFNN),^{44–46} which was used throughout this study with forecasting horizon and supervised learning.

ANNs are composed of neurons that are distributed between layers: one input layer, intermediate or hidden lay-

ers, and one output layer.^{41,47} A single neuron computes the sum of its inputs, adds a bias term, and drives the result through a generally nonlinear activation function to produce a single output termed the activation level of the neuron.⁴⁸ The input layer receives inputs (x_i) from the real world and each succeeding layer receives weighted outputs ($w_{ij} \times x_i$) from the preceding layer as its input, thus resulting in a feedforward artificial neural network (ANN), in which each input is fed forward to its succeeding layer where it is treated. The outputs of the previous layer constitute the outputs to the real world.^{49,50} A continuous multivariable function $F(x)$ is approached in the neural network by a selected function $f(x,w)$ for a fixed number of input variables

$$x = (x_0; x_1, \dots, x_l) \quad (1)$$

and w is an array of weights, defined below. $x_0 = 1$ is the constant input, called *bias*, that is used to simulate thresholding effects in the neuron, and which also serves to simplify the mathematics; x_i , $i = 1, \dots, l$ are neural network inputs, and l is the number of input nodes.

The output from the hidden layer is

$$y = (y_0; y_1, \dots, y_m) \quad (2)$$

where $y_0 = 1$ is the constant output from the bias neuron, m is the number of processing elements in the hidden layer, and y_j is output from the j -th processing element of the hidden layer.

$$y_j = f \left(\sum_{i=0}^l w_{ji}^0 x_i \right), j = 1, \dots, m \quad (3)$$

w_{ji}^0 is a weight associated with a connection between the i -th processing element in the input layer and the j -th processing element in the hidden layer. For bias, the weight w_{j0}^0 is taken as equal to 1. The formula for the output layer of the neural network is like that in Eq. (3), only the signal from the bias neuron does not exist:

$$z = (z_1; z_2, \dots, z_n) \quad (4)$$

where

$$z_k = f \left(\sum_{j=0}^m w_{kj}^1 y_j \right), k = 1, \dots, n \quad (5)$$

n is the number of output neurons, and w_{kj}^1 is weight associated with a connection between the j -th processing element in the hidden layer and the k -th processing element in the output layer. For bias, the weight w_{k0}^1 is again taken as equal to 1.⁵¹ The output is computed by means of a transfer function, also called the activation function.⁵⁰

Hyperbolic tangent sigmoid transfer function:

$$f(a) = \frac{e^a - e^{-a}}{e^a + e^{-a}} \quad (6)$$

Logarithmic sigmoid transfer function:

$$f(a) = \frac{1}{1 + e^{-a}} \quad (7)$$

Pure linear transfer function:

$$f(a) = a \quad (8)$$

The methodology of ANN application can be divided into three steps: training, validation, and generalization. During training, the synaptic and bias weights that were chosen randomly at the beginning of the training, are optimized using a set of data that can either be generated experimentally or it can originate from validated models.^{41,52} The only part of the available data is used for the training of the neural network. Different subsets of data are used for validating and generalizing the model previously trained. The efficiency of the ANN depends on several factors, like the number of neurons, the number of hidden layers, and the transfer function is chosen. Usually, the number of neurons in the input and output layers corresponds to the number of input and output variables. The number of neurons in the hidden layer must be chosen carefully, because on the one hand, networks with few neurons tend to have low precision, and on the other hand, an excessively high number of neurons can lead to overfitting which in turn results in problems of generalization of the model.^{41,53} The outputs from the output layer comprise a prediction of the dependent variables of the model. The network learns the relationships between the independent and dependent variables by iterative comparison of the predicted outputs and experimental outputs, and subsequent adjustment of the weight matrix and bias vector of each layer by a back-propagation training algorithm. Hence, the network progresses an NN model capable of predicting with acceptable accuracy the output variables lying within the model space defined by the training set. Consequently, the objective of ANN modelling is to minimize the prediction errors of validation data presented to the network after completion of the training step.⁵⁰

2.2 Modelling procedure

A procedure based on the design and optimization of the architecture of the neural network was used, as described further:

- Data collection and division
 - DB1 for pure CO₂.
 - DB2 for pure CH₄.
 - DB3 for pure N₂.
 - DB4 for (CO₂, CH₄) binary mixture.
 - DB5 for (CO₂, N₂) binary mixture.
 - DB6 for (CH₄, N₂) binary mixture.
 - DB7 for (CO₂, CH₄, and N₂) ternary mixture.
- Choice of parameters of neural networks.
- NN creation.
 - Training algorithm (BFGS).

- Neurons in the hidden layer (3-20).
 - Activation functions in the hidden and output layer (logsig, tansig, exponential, and purelin).
- Saving NN parameters.

2.3 Database collection

The collected data were imported from different works in the literature in order to study the adsorption phenomena of pure gases (CO₂, CH₄, and N₂), their binary mixtures, and their ternary mixtures on different activated carbons (Table 1).^{2,9,33,54–63}

Table 1 – Experimental database

Database	Samples	References
DB1	CO ₂	54, 55, 56, 57, 58, 59, 61, 2, 9, 62
DB2	CH ₄	54, 61, 55, 2, 63, 9, 33, 59, 57, 56, 62, 60
DB3	N ₂	54, 55, 33, 57, 60
DB4	(CO ₂ , CH ₄)	54, 55, 9, 62
DB5	(CO ₂ , N ₂)	54, 55
DB6	(CH ₄ , N ₂)	54, 55
DB7	(CO ₂ , CH ₄ , N ₂)	54

Table 2 – Database size

Database (DB)	Neural Network	Database size
DB1	NN1	417
DB2	NN2	625
DB3	NN3	143
DB4	NN4	87
DB5	NN5	64
DB6	NN6	64
DB7	NN7	40

For each database (DB1, DB2, DB3, DB4, DB5, DB6, and DB7) (Table 2), a set of input variables were identified. For DB1, DB2, and DB3, the inputs were the characteristics of activated carbons (specific surface area and micropore volume), and the operating conditions (temperature and pressure). For DB4, DB5, and DB6, the inputs were the average molar masses of mixtures, characteristics of activated carbons, and the operating conditions. The average molar masses of mixtures was calculated by the following equation:

$$M = \sum_{i=1}^n x_i M_i \quad (9)$$

where M_i [g mol⁻¹] is the molar mass of component i , and x_i is the molar fraction of component i .⁶¹ For DB7, the inputs

were the average molar mass of mixture and the pressure. The outputs of DB1, DB2, and DB3 were the adsorption amounts of compounds (Q_1 for CO_2), (Q_2 for CH_4), and (Q_3 for N_2); respectively. The outputs of DB4, DB5, and DB6 were the adsorption amounts of each compound: (Q_1, Q_2) for DB4, (Q_1, Q_3) for DB5, and (Q_2, Q_3) for DB6. For DB7, the outputs were the adsorption amounts of each compound (Q_1, Q_2 , and Q_3). The values of standard deviations (STD) and mean for the inputs and outputs data are shown in (Table 3).

2.4 Model development

The samples were split randomly into three subsets: 60 % for the training phase, 20 % for the validation phase, and 20 % for the test phase. The networks were trained us-

ing the quasi-Newton BFGS (Broyden-Fletcher-Goldfarb-Shanno) algorithm (trainbfg). The FFNNs contained three layers of neurons or nodes: one input layer with four neurons for (NN1, NN2, and NN3), five neurons for (NN4, NN5, and NN6), two neurons for NN7, and one hidden layer with a number of active neurons optimized during training. In addition, one output layer with one neuron for (NN1, NN2, and NN3), two neurons for (NN4, NN5, and NN6), and three neurons for NN7. The number of hidden neurons varied from 3 to 20 neurons. The tangent sigmoid (tansig), the log sigmoid (logsig), the pure linear (purelin), and the exponential transfer functions were used in the hidden and the output layer.

The ANN modelling of the adsorption of gas mixtures on activated carbons was performed using STATISTICA software (version 8.0).

Table 3 – Statistical analysis of input and output data

Data Bases	Inputs and outputs	STD	Mean
DB1 Pure (CO_2)	specific surface area/ $\text{m}^2 \text{g}^{-1}$	700.7141	1364.90
	micropore volume/ $\text{cm}^3 \text{g}^{-1}$	0.3445	0.5817
	T/K	18.1164	311.3843
	p/MPa	1.7845	1.0175
	$Q_1/\text{mmol g}^{-1}$	5.0907	5.5306
DB2 Pure (CH_4)	specific surface area/ $\text{m}^2 \text{g}^{-1}$	465.9869	1211.40
	micropore volume/ $\text{cm}^3 \text{g}^{-1}$	0.1911	0.4971
	T/K	25.6785	305.5740
	p/MPa	1.9516	1.0565
	$Q_2/\text{mmol g}^{-1}$	2.1273	2.4958
DB3 Pure (N_2)	specific surface area/ $\text{m}^2 \text{g}^{-1}$	309.0018	861.1189
	micropore volume/ $\text{cm}^3 \text{g}^{-1}$	0.0863	0.3957
	T/K	11.0189	315.8290
	p/MPa	3.8065	2.4823
	$Q_3/\text{mmol g}^{-1}$	1.2209	1.4928
DB4 (CO_2 - CH_4) binary mixture	specific surface area/ $\text{m}^2 \text{g}^{-1}$	213.6416	1080
	micropore volume/ $\text{cm}^3 \text{g}^{-1}$	0.1128	0.4915
	average molar mass/ g mol^{-1}	6.2345	29.5084
	T/K	14.9291	314.5109
	p/MPa	3.5611	4.050
	$Q_1/\text{mmol g}^{-1}$	2.6747	4.1178
	$Q_2/\text{mmol g}^{-1}$	1.3985	2.2096
DB5 (CO_2 - N_2) binary mixture	specific surface area/ $\text{m}^2 \text{g}^{-1}$	201.0354	1004.5
	micropore volume/ $\text{cm}^3 \text{g}^{-1}$	0.1073	0.4525
	average molar mass/ g mol^{-1}	3.8858	36.1589
	T/K	9.8566	310.6250
	p/MPa	3.7776	4.9866
	$Q_1/\text{mmol g}^{-1}$	2.9320	4.6797
	$Q_3/\text{mmol g}^{-1}$	0.7569	1.0029
DB6 (CH_4 - N_2) binary mixture	specific surface area/ $\text{m}^2 \text{g}^{-1}$	201.0354	1004.5
	micropore volume/ $\text{cm}^3 \text{g}^{-1}$	0.1073	0.4525
	average molar mass/ g mol^{-1}	2.9658	22.3852
	T/K	9.8566	310.6250
	p/MPa	3.7496	4.9644
	$Q_2/\text{mmol g}^{-1}$	1.6294	2.6811
	$Q_3/\text{mmol g}^{-1}$	0.8801	1.2351
DB7 (CO_2 - CH_4 - N_2) ternary mixture	average molar mass/ g mol^{-1}	2.5605	25.2276
	p/MPa	2.0303	2.6867
	$Q_1/\text{mmol g}^{-1}$	1.7813	2.7056
	$Q_2/\text{mmol g}^{-1}$	1.3327	2.8153
	$Q_3/\text{mmol g}^{-1}$	0.6007	0.7464

Table 4 – Structure of the optimized ANN model

NN models	Training algorithm	Input layer	Hidden layer		Output layer	
		neuron number	neuron number	activation function	neuron number	activation function
NN1	BFGS algorithm quasi-Newton (trainbfg)	4	16	Tansig	1	Tansig
NN2	BFGS algorithm quasi-Newton (trainbfg)	4	17	Tansig	1	Logsig
NN3	BFGS algorithm quasi-Newton (trainbfg)	4	13	Tansig	1	Tansig
NN4	BFGS algorithm quasi-Newton (trainbfg)	5	13	Tansig	2	Logsig
NN5	BFGS algorithm quasi-Newton (trainbfg)	5	8	Logsig	2	Identity
NN6	BFGS algorithm quasi-Newton (trainbfg)	5	11	Tansig	2	Identity
NN7	BFGS algorithm quasi-Newton (trainbfg)	2	9	Tansig	3	Tansig

3 Results and discussion

The definitive goal of this investigation was to test the ability of artificial neural network architectures with the least number of parameters to represent a wide variety of isotherm data. The input vectors had 417, 625, 143, 87, 64, 64, 40 set of experimental data for NN1 to NN7; respectively. The input layers contain:

- Four neurons for (NN1, NN2, and NN3), representing the specific surface area and the micropore volume of activated carbons, temperature, and pressure.
- Five neurons for (NN4, NN5, NN6), representing average molar mass, specific surface area, and micropore volume of activated carbons, temperature, and pressure.
- Two neurons for NN7, representing the average molar mass of mixture, and pressure.

The output layer has one neuron for (NN1, NN2, and NN3), two neurons for (NN4, NN5, NN6), and three neurons for NN7. ANNs contain one hidden layer and feedforward was used for training the input data. The quasi-Newton's algorithm BFGS was used for estimating the parameters of the ANNs model. Table 4 shows the structure of the optimized NN models.

According to the previous discussion, seven neural network models were developed with the aim of predicting the adsorption of gases (CO_2 , CH_4 , and N_2) by activated carbons. Figs. 1–7 show a comparison between the predicted and experimental values of the outputs variables for the entire dataset by using the neural network models (NN1 to NN7). The plot and the parameters of the linear regression were obtained using the MATLAB function "plotregression". Figs. 1–7 show the agreement plots for the adsorption amount with agreement vectors approaching the ideal for the entire data set for NN1 to NN7, respectively.

- For NN1, $[\alpha, \beta, R] = [0.99, 0.071, 0.99656]$;
- For NN2, $[\alpha, \beta, R] = [0.97, 0.083, 0.99284]$;
- For NN3, $[\alpha, \beta, R] = [0.97, 0.028, 0.99388]$;

- For NN4, $[\alpha, \beta, R] = [0.99, 0.11, 0.99639]$ for Q_1 and $[\alpha, \beta, R] = [0.94, 0.13, 0.99472]$ for Q_2 ;
- For NN5, $[\alpha, \beta, R] = [1, 0.015, 0.99716]$ for Q_1 and $[\alpha, \beta, R] = [0.99, 0.0096, 0.99572]$ for Q_3 ;
- For NN6, $[\alpha, \beta, R] = [1, -0.00058, 0.99746]$ for Q_2 and $[\alpha, \beta, R] = [1, 0.0065, 0.99783]$ for Q_3 ;
- For NN7, $[\alpha, \beta, R] = [0.97, 0.041, 0.9946]$ for Q_1 and $[\alpha, \beta, R] = [1, 0.032, 0.99089]$ for Q_2 and $[\alpha, \beta, R] = [0.92, 0.039, 0.9947]$ for Q_3 .

Most points are situated very near the diagonal. Figs. 1–7 show an excellent agreement between the experimental data and the ANNs predicted results for adsorption.

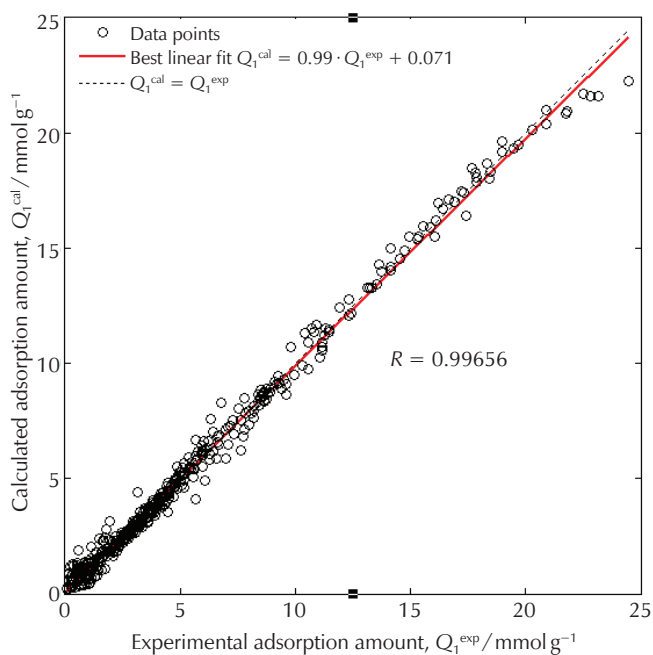


Fig. 1 – Comparison of experimental and calculated values for the entire data set of NN1

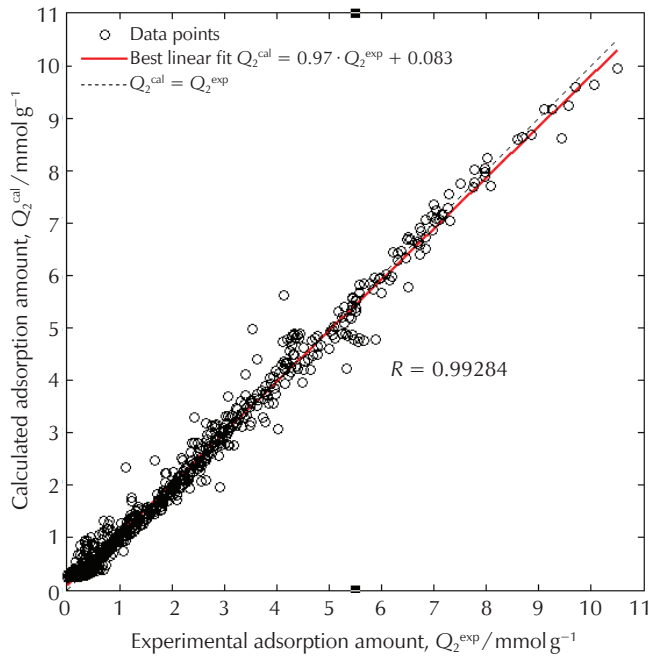


Fig. 2 – Comparison of experimental and calculated values for the entire data set of NN2

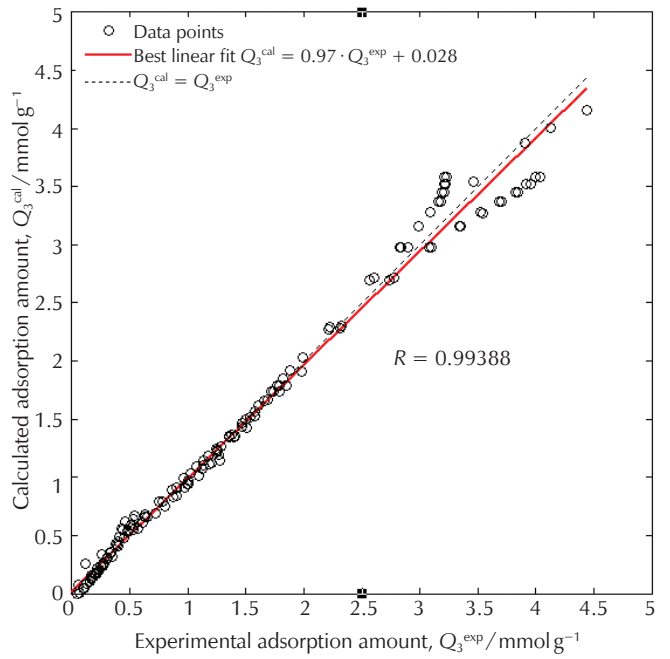


Fig. 3 – Comparison of experimental and calculated values for the entire data set of NN3

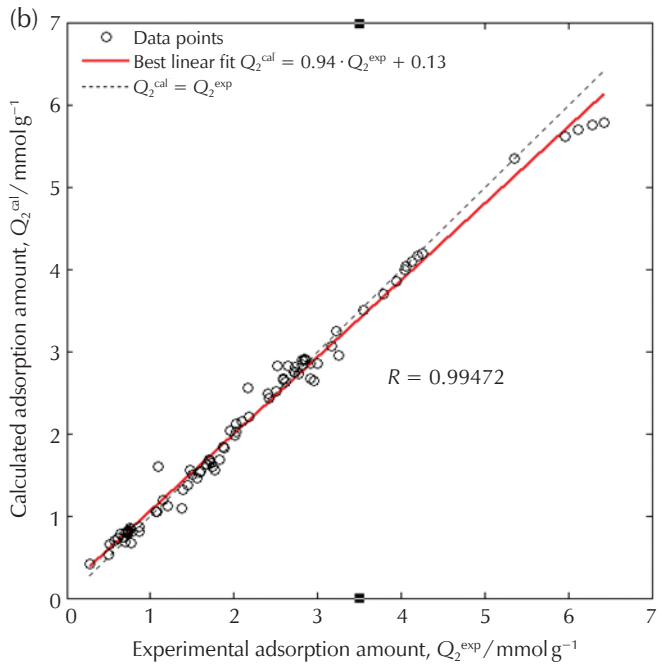
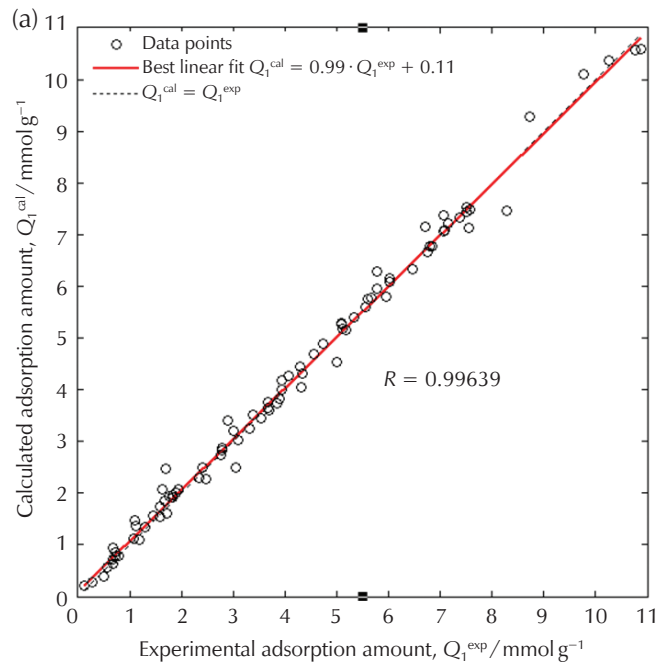


Fig. 4 – Comparison of experimental and calculated values for the entire data set of NN4 (a) Q_1 , (b) Q_2

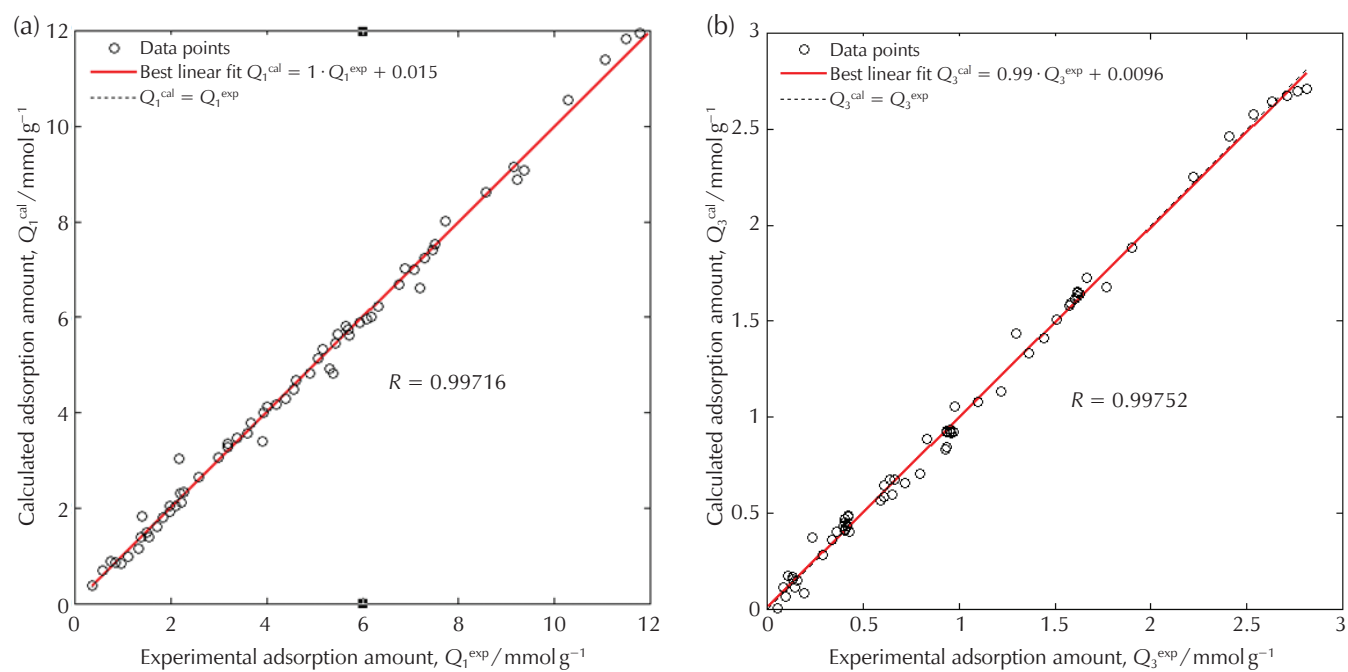


Fig. 5 – Comparison of experimental and calculated values for the entire data set of NN5 (a) Q_1 , (b) Q_3

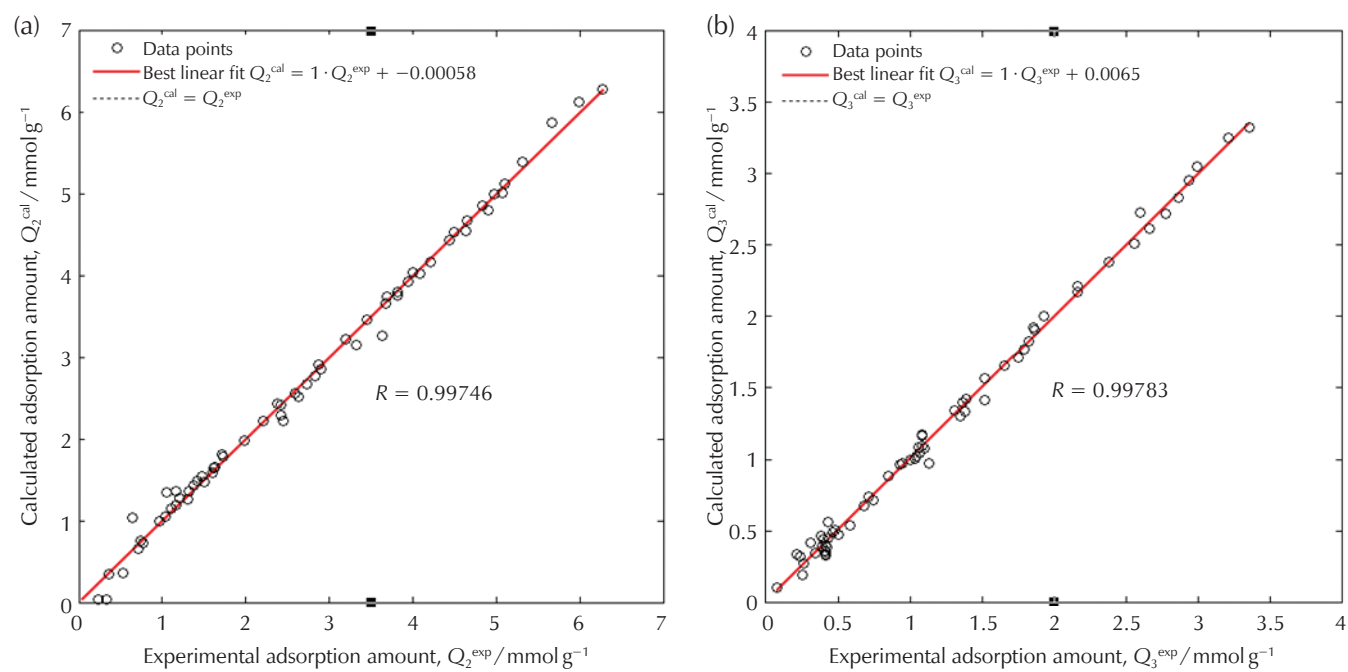


Fig. 6 – Comparison of experimental and calculated values for the entire data set of NN6 (a) Q_2 , (b) Q_3

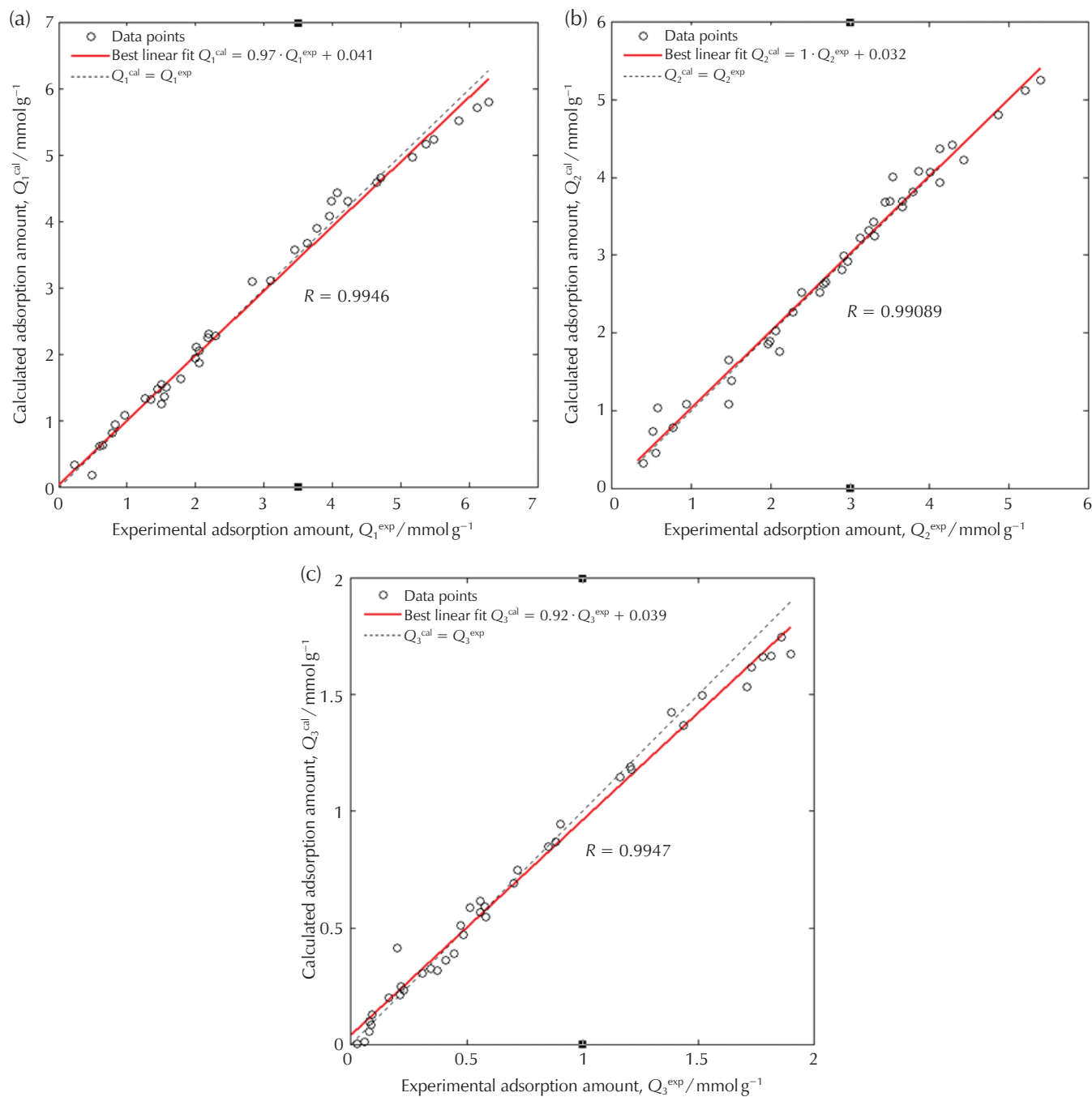


Fig. 7 – Comparison of experimental and calculated values for the entire data set of NN7 (a) Q_1 , (b) Q_2 , and (c) Q_3

Table 5 shows the vectors of linear regression for the neural models (NN1, NN2, NN3, NN4, NN5, NN6, and NN7). Clearly, the proposed neuronal approach gives satisfactory results with regression vector values approaching the ideal [i.e., $\alpha = 1$ (slope), $\beta = 0$ (y intercept), $R = 1$ (correlation coefficient)] in the adjustment of the profiles of Q_1 , Q_2 , and Q_3 .

The performances of various sub-models were estimated in terms of the root mean squared error (RMSE) criterion. The RMSE was calculated using Eq. (10).⁴⁴

$$\text{RMSE} = \sqrt{\frac{\sum_{i=1}^n (Y_{i,\text{exp}} - Y_{i,\text{cal}})^2}{n}} \quad (10)$$

where n is the total number of data points; $Y_{i,\text{exp}}$ is the experimental value, $Y_{i,\text{cal}}$ represents the calculated value from the neural network models.

Table 5 – Linear regression vectors [linear equation: $Y^{cal} = \alpha Y^{exp} + \beta$, with α = splote, β = y intercept, R = correlation coefficient]

NN	Outputs	Datasets	α	β	R	RMSE
NN1	Q_1	training phase	0.99	0.045	0.99716	0.3802
		validation phase	0.97	0.14	0.99553	0.5344
		test phase	0.99	0.065	0.99604	0.4194
		total	0.99	0.077	0.99656	0.4229
NN2	Q_2	training phase	0.98	0.073	0.99322	0.2472
		validation phase	0.97	0.12	0.99038	0.2943
		test phase	0.97	0.076	0.99422	0.2394
		total	0.97	0.083	0.99284	0.2558
NN3	Q_3	training phase	0.98	0.02	0.99407	0.1333
		validation phase	0.95	0.03	0.99566	0.1143
		test phase	0.95	0.056	0.9925	0.1631
		total	0.97	0.028	0.99388	0.1363
NN4	Q_1	training phase	0.98	0.077	0.99639	0.2322
		validation phase	1	0.14	0.99458	0.2366
		test phase	0.99	0.18	0.99651	0.2249
		total	0.99	0.11	0.99639	0.2317
	Q_2	training phase	0.96	0.078	0.99332	0.1417
		validation phase	0.92	0.17	0.99691	0.1902
		test phase	0.91	0.17	0.99604	0.1860
		total	0.94	0.13	0.99472	0.1614
NN5	Q_1	training phase	0.99	0.068	0.99598	0.2519
		validation phase	1	-0.068	0.99949	0.1764
		test phase	0.97	0.07	0.99911	0.1210
		total	1	0.015	0.99716	0.2197
	Q_3	training phase	0.99	0.0031	0.99705	0.0531
		validation phase	1	0.025	0.99786	0.0563
		test phase	0.98	0.0047	0.99875	0.0492
		total	0.99	0.0096	0.99752	0.0530
NN6	Q_2	training phase	0.98	0.036	0.9966	0.1278
		validation phase	1.1	-0.17	0.99883	0.1240
		test phase	0.99	0.038	0.99987	0.0360
		total	1	-0.00058	0.99746	0.1155
	Q_3	training phase	0.99	0.016	0.99795	0.0594
		validation phase	1	0.0087	0.99725	0.0601
		test phase	1	-0.062	0.99953	0.0413
		total	1	0.0065	0.99783	0.0578
NN7	Q_1	training phase	0.96	0.077	0.99439	0.1855
		validation phase	1.1	-0.16	0.99447	0.2184
		test phase	0.93	0.15	0.99929	0.1555
		total	0.97	0.041	0.9946	0.1871
	Q_2	training phase	0.99	0.027	0.9967	0.1106
		validation phase	0.95	0.19	0.99069	0.2250
		test phase	1.4	-1	0.9951	0.2711
		total	1	0.032	0.99089	0.1794
	Q_3	training phase	0.97	0.014	0.9968	0.0391
		validation phase	0.88	0.091	0.99352	0.1039
		test phase	0.91	0.0022	0.99812	0.1146
		total	0.92	0.039	0.9947	0.0755

3.1 Comparisons between ANN models and classical models

3.1.1 Comparison between ANN models and the Gibbs model for the prediction of pure gases (CO_2 , CH_4 , and N_2) adsorption

The Gibbs model was previously tested for predicting the adsorption of pure gases (CO_2 , CH_4 , and N_2) on activated carbon at 318.2 K.⁵⁵ Experimental results were compared

with Gibbs model and ANN models in terms of the mean absolute error (MAE), the model predictive error (MPE), the root mean squared error (RMSE), and the standard error of prediction (SEP). The MAE, MPE, and SEP are defined as follows:⁶⁴⁻⁶⁷

$$MAE = \frac{1}{n} \sum_{i=1}^n |(y_{i,exp} - y_{i,cal})| \quad (11)$$

$$\text{MPE}(\%) = \frac{100}{n} \sum_{i=1}^n \left| \frac{y_{i,\text{exp}} - y_{i,\text{cal}}}{y_{i,\text{exp}}} \right| \quad (12)$$

$$\text{SEP}(\%) = \frac{\text{RMSE}}{y_e} \quad (13)$$

where n is the total number of data points; $y_{i,\text{exp}}$ is the experimental value, $y_{i,\text{cal}}$ is the calculated value from the neural network models or Gibbs model, and y_e is the mean value of experimental data.

Table 6 – Comparison of the NN models and the Gibbs model for the adsorption of pure gases

Errors	CO ₂		CH ₄		N ₂	
	$n = 26$		$n = 21$		$n = 22$	
	NN1	Gibbs	NN2	Gibbs	NN3	Gibbs
MPE	1.6778	22.2812	8.8424	12.2306	6.2641	10.4138
RMSE	0.1413	2.7507	0.4547	0.7817	0.2584	0.4535
SEP	0.0196	0.3816	0.1009	0.1734	0.0850	0.1491
MAE	0.1150	1.8792	0.3928	0.6289	0.2097	0.3690

Table 6 shows the comparison between NN models and the Gibbs model for the prediction of the adsorption isotherm of pure gases (CO₂, CH₄, and N₂). The NN models developed in this work for the adsorption of pure gases (CO₂, CH₄, and N₂), gave lower errors than the Gibbs model.

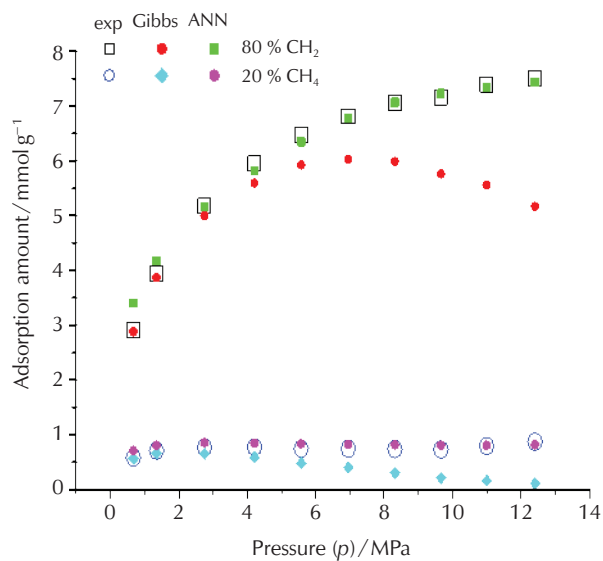


Fig. 9 – Nitrogen/CO₂ adsorption on dry activated carbon at 318.2 K. Prediction of the data with Gibbs isotherm and ANN.

3.1.2 Comparison between ANN models and the Gibbs model for the prediction of binary mixtures (CO₂, CH₄), (CO₂, N₂), and (CH₄, N₂) adsorption

Figs. 8–10 present the comparison between theory (NN models, Gibbs model) and experimental data of the adsorption isotherms for temperature $T = 318.2$ K of binary mixtures (CO₂, CH₄), (CO₂, N₂), and (CH₄, N₂) in real units with composition of (80, 20), (80, 20), and (60, 40), respectively.⁵⁵ Figs. 8, 9, 10 show better agreement of experimental data with NN model than the Gibbs model.

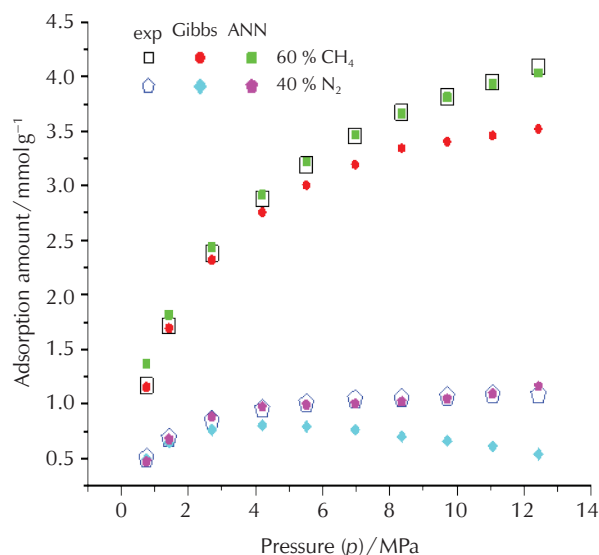


Fig. 8 – Methane/CO₂ adsorption on dry activated carbon at 318.2 K. Prediction of the data with Gibbs isotherm and ANN

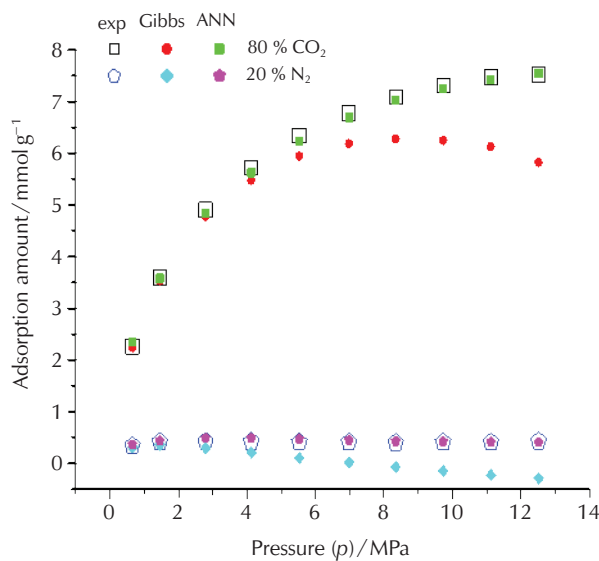


Fig. 10 – Methane/nitrogen adsorption on dry activated carbon at 318.2 K. Prediction of the data with Gibbs isotherm and ANN.

3.1.3 Comparison between ANN model, the Generalized dual-site Langmuir model, and the IAST theory for the prediction of the adsorption of ternary mixture (CO₂, CH₄, and N₂)

The generalized dual-site Langmuir model and the IAST theory were previously tested for the prediction of the adsorption of ternary mixture (CO₂, CH₄, N₂) by F. Dreisbach et al.⁵⁴ In this work, the comparison between models (generalized dual-site Langmuir model, IAST theory, and NN model) and the experimental data of the adsorption isotherm of the ternary mixture (CO₂, CH₄, and N₂) on activated carbon (AC) is presented. The mean relative deviations between the predicted ($n = n_1 + n_2 + n_3$) and the experimental (n_{exp}) total amounts adsorbed, as well as between the predicted ($x_1 = n_1/(n_1 + n_2 + n_3)$) and measured concentration ($x_{1,\text{exp}}$) of component 1 in the ternary mixture are calculated as:

$$\Delta n = \frac{1}{N} \sum_{i=1}^N \sqrt{\left(\frac{n_{\text{exp},i} - n_i}{n_{\text{exp},i}} \right)^2} \quad (14)$$

$$\Delta x_1 = \frac{1}{N} \sum_{i=1}^N \sqrt{\left(\frac{x_{1,\text{exp},i} - x_{1,i}}{x_{1,\text{exp},i}} \right)^2} \quad (15)$$

with N being the total number of measurements.⁵⁴ The resulting deviations are given in Table 7.

Table 7 – Mean relative deviations between predicted and measured ternary gas mixture adsorption equilibria on the AC Norit R1 at $T = 298$ K

	Generalized dual-site Langmuir	IAST	ANN
Δn %	4.88	4.29	3.18
Δx_1 %	15.11	27.21	9.91
Δx_2 %	10.79	14.85	7.22
Δx_3 %	35.53	47.19	13.06

The NN model developed in this work for the prediction of the adsorption of the ternary mixture (CO₂, CH₄, and N₂) gave lower errors than the generalized dual-site Langmuir model than IAST. This indicates that the neural network model is successful in the prediction of the ternary mixture of (CO₂, CH₄, and N₂) adsorption isotherm.

4 Conclusion

Artificial neural networks were proposed to model pure, binary, and ternary gas mixtures adsorption equilibria.

Feedforward ANN models were applied to seven systems (pure CO₂, CH₄, N₂, their binary mixtures, and their ternary mixture). Of the total data, 60 %, 20 %, and 20 % were used, respectively, for training, validation, and testing of the seven models. The networks were trained using the quasi-Newton BFGS (Broyden-Fletcher-Goldfarb-Shanno) algorithm. The developed ANNs showed an accurate prediction of experimental data with root mean square errors of 0.4229 for NN1, 0.2558 for NN2, 0.1363 for NN3, 0.2317 for Q₁ for NN4, 0.1614 for Q₂ for NN4, 0.2197 for Q₁ for NN5, 0.0530 for Q₃ for NN5, 0.1155 for Q₂ for NN6, 0.0578 for Q₃ for NN6, 0.1871 for Q₁ for NN7, 0.1794 for Q₂ for NN7, and 0.0755 for Q₃ for NN7. In this study, the Gibbs model was also used to study the equilibrium data for pure (CO₂, CH₄, and N₂), and their binary mixtures. The generalized dual-site Langmuir model and the IAST theory were used to examine the equilibrium data of the ternary mixture of (CO₂, CH₄, and N₂). The comparison of the results of the ANNs models and classical models indicated that the ANN predicted gas adsorption on AC more accurately than the classical models over the full range of operating conditions.

List of abbreviations

- AC – activated carbon
- ANN – artificial neural network
- BFGS – Broyden-Fletcher-Goldfarb-Shanno
- Cal – calculated
- DB – database
- Exp – experimental
- FFNN – feedforward neural network
- IAST – Ideal adsorption solution theory
- Logsig – logarithmic sigmoid transfer function
- MAE – mean absolute error
- MPE – model predictive error
- MSE – mean square error
- NN – neural network
- Purelin – pure linear transfer function
- Q₁ – adsorption amount of CO₂
- Q₂ – adsorption amount of CH₄
- Q₃ – adsorption amount of N₂
- R – correlation coefficient
- RMSE – root mean squared error
- RSM – response surface methodology
- SEP – standard error of prediction
- SLD – simplified local density
- STD – standard deviations
- Tansig – hyperbolic tangent sigmoid transfer function

References

Literatura

1. N. Álvarez-Gutiérrez, M. V. Gil, F. Rubiera, C. Pevida, Kinetics of CO₂ adsorption on cherry stone-based carbons in CO₂/CH₄ separations, *Chem. Eng. J.* **307** (2017) 249–257, doi: <https://doi.org/10.1016/j.cej.2016.08.077>.
2. L. Zhou, J. Wu, M. Li, Q. Wu, Y. Zhou, Prediction of multi-component adsorption equilibrium of gas mixtures including supercritical components, *Chem. Eng. Sci.* **60** (2005) 2833–2844, doi: <https://doi.org/10.1016/j.ces.2004.11.058>.
3. S. Qiao, K. Wang, X. Hu, Using local IAST with micropore size distribution to predict multicomponent adsorption equilibrium of gases in activated carbon, *Langmuir*. **16** (3) (2000) 1292–1298, doi: <https://doi.org/10.1021/la990785q>.
4. G. Morse, R. Jones, J. Thibault, F. H. Tezel, Neural network modelling of adsorption isotherms, *Adsorption*. **17** (2010) 303–309, doi: <https://doi.org/10.1007/s10450-010-9287-1>.
5. S. Beutekamp, P. Harting, Experimental determination and analysis of high pressure adsorption data of pure gases and gas mixtures, *Adsorption*. **8** (2002) 255–269, doi: <https://doi.org/10.1023/A:1021548112040>.
6. C. J. King, *Separation Processes*, Center for Studies in Higher Education, 1980.
7. S. Rebouh, M. Bouhedda, S. Hanini, Neuro-fuzzy modeling of Cu(II) and Cr(VI) adsorption from aqueous solution by wheat straw, *Desalin. Water Treat.* **57** (14) (2016) 6515–6530, doi: <https://doi.org/10.1080/19443994.2015.1009171>.
8. A. Dong, J. Xie, W. Wang, L. Yu, Q. Liu, Y. Yin, A novel method for amino starch preparation and its adsorption for Cu(II) and Cr(VI), *J. Hazard. Mater.* **181** (1-3) (2010) 448–454, doi: <https://doi.org/10.1016/j.jhazmat.2010.05.031>.
9. V. Goetz, O. Pupier, A. Guillot, Carbon dioxide-methane mixture adsorption on activated carbon, *Adsorption*. **12** (2006) 55–63, doi: <https://doi.org/10.1007/s10450-006-0138-z>.
10. H. Yi, F. Li, P. Ning, X. Tang, J. Peng, Y. Li, H. Deng, Adsorption separation of CO₂, CH₄, and N₂ on microwave activated carbon, *Chem. Eng. J.* **215-216** (2013) 635–642, doi: <https://doi.org/10.1016/j.cej.2012.11.050>.
11. A. Rostami, M. A. Anabaz, H. R. E. Gahrooei, M. Arabloo, A. Bahadori, Accurate estimation of CO₂ adsorption on activated carbon with multi-layer feed-forward neural network (MLFNN) algorithm, *Egypt. J. Petrol.* **27** (2018) 65–73, doi: <https://doi.org/10.1016/j.ejpe.2017.01.003>.
12. E. N. El Qada, S. J. Allen, G. M. Walker, Influence of preparation conditions on the characteristics of activated carbons produced in laboratory and pilot scale systems, *Chem. Eng. J.* **142** (2008) 1–13, doi: <https://doi.org/10.1016/j.cej.2007.11.008>.
13. S. Jribi, T. Miyazaki, B. B. Saha, A. Pal, M. M. Younes, S. Koyama, A. Maalej, Equilibrium and kinetics of CO₂ adsorption onto activated carbon, *Int. J. Heat Mass Transf.* **108** (2017) 1941–1946, doi: <https://doi.org/10.1016/j.ijheatmasstransfer.2016.12.114>.
14. Z. Zhang, W. Zhang, X. Chen, Q. Xia, Z. Li, Adsorption of CO₂ on zeolite 13X and activated carbon with higher surface area, *Sep. Sci. Techno.* **45** (5) (2010) 710–719, doi: <https://doi.org/10.1080/01496390903571192>.
15. Y. Belmabkhout, R. Serna-Guerrero, A. Sayari, Adsorption of CO₂ from dry gases on MCM-41 silica at ambient temperature and high pressure. 1: Pure CO₂ adsorption, *Chem. Eng. Sci.* **64** (2009) 3721–3728, doi: <https://doi.org/10.1016/j.ces.2009.03.017>.
16. B. J. Maring, P. A. Webley, A new simplified pressure/vacuum swing adsorption model for rapid adsorbent screening for CO₂ capture applications, *Int. J. Greenhouse. Gas. Control.* **15** (2013) 16–31, doi: <https://doi.org/10.1016/j.ijggc.2013.01.009>.
17. K. S. Hwang, S. Y. Gong, W. K. Lee, Adsorption equilibria for hydrogen and carbon dioxide on activated carbon at high pressure up to 30 atm, *Kor. J. Chem. Eng.* **8** (1991) 148–155, doi: <https://doi.org/10.1007/BF02706676>.
18. I. Langmuir, The adsorption of gases on plane surfaces of glass, mica and platinum, *J. Amer. Chem. Soc.* **40** (1918) 1361–1403, doi: <https://doi.org/10.1021/ja02242a004>.
19. H. Freundlich, Über die adsorption in lösungen, *Z. Phys. Chem.* **57U** (1907) 385–470, doi: <https://doi.org/10.1515/zpch-1907-5723>.
20. R. Sips, On the structure of a catalyst surface, *J. Chem. Phys.* **16** (1948) 490–495, doi: <https://doi.org/10.1063/1.1746922>.
21. J. Toth, State equations of the solid gas interface layer, *Acta Chem. Acad. Hung.* **69** (1971) 311–317.
22. D. M. Ruthven, *Principles of Adsorption and Adsorption Processes*, Wiley, New York, 1984, doi: <https://doi.org/10.1002/aic.690310335>.
23. R. T. Yang, *Gas Separation by Adsorption Processes*, Butterworths, Boston, 1987.
24. D. D. Do, *Adsorption Analysis: Equilibria and Kinetics*, Imperial College Press, London, 1998, doi: <https://doi.org/10.1142/9781860943829>.
25. J. A. Schwarz, C. L. Contescu, *Surfaces of Nanoparticles and Porous Materials*. Vol. 78, Marcel Dekker Inc., New York, 1999, pp. 392, doi: <https://doi.org/10.1201/9780824746681>.
26. A. L. Myers, J. M. Prausnitz, Thermodynamics of mixed-gas adsorption, *A. I. Ch. E. J.* **11** (1965) 121–127, doi: <https://doi.org/10.1002/aic.690110125>.
27. S. Suwanayuen, R. P. Danner, A gas adsorption isotherm equation based on vacancy solution theory, *A. I. Ch. E. J.* **26** (1980) 68–76, doi: <https://doi.org/10.1002/aic.690260112>.
28. S. Suwanayuen, R. P. Danner, Vacancy solution theory of adsorption from gas mixtures, *A. I. Ch. E. J.* **26** (1980) 76–83, doi: <https://doi.org/10.1002/aic.690260113>.
29. T. W. Cochran, R. L. Kabel, R. P. Danner, Vacancy solution theory of adsorption using Flory–Huggins activity coefficient equations, *A. I. Ch. E. J.* **31** (1985) 268–277, doi: <https://doi.org/10.1002/aic.690310214>.
30. D. M. Ruthven, K. F. Loughlin, K. A. Holborow, Multicomponent sorption equilibrium in molecular sieve zeolites, *Chem. Eng. Sci.* **28** (1973) 701–709, doi: [https://doi.org/10.1016/0009-2509\(77\)80004-3](https://doi.org/10.1016/0009-2509(77)80004-3).
31. D. M. Ruthven, F. Wong, Generalized statistical model for the prediction of binary adsorption equilibria in zeolites, *Ind. Eng. Chem. Fund.* **24** (1984) 27–32, doi: <https://doi.org/10.1021/i100017a005>.
32. R. J. Grant, M. Manes, Adsorption of binary hydrocarbon gas mixtures on activated carbon, *Ind. Eng. Chem. Fund.* **5** (1966) 490–498, doi: <https://doi.org/10.1021/i160020a010>.
33. M. Hasanzadeh, M. R. Dehghani, F. Feyzi, B. Behzadi, A new simplified local density model for adsorption of pure gases and binary mixtures, *Int. J. Thermophys.* **31** (2010) 2425–2439, doi: <https://doi.org/10.1007/s10765-010-0827-4>.
34. A. Ghosh, P. Das, K. Sinha, Modeling of biosorption of Cu(II) by alkali-modified spent tea leaves using response surface methodology (RSM) and artificial neural network (ANN), *Appl. Water. Sci.* **5** (2015) 191–199, doi: <https://doi.org/10.1007/s13201-014-0180-z>.
35. Z. Shahryari, A. Sharifi, A. Mohebbi, Artificial neural network (ANN) approach for modeling and formulation of phenol adsorption onto activated carbon, *J. Eng. Thermo-*

- phys. **22** (2013) 322–336, doi: <https://doi.org/10.1134/S181023281304005X>.
36. A. B. *Bulsari*, A. *Palosaari*, Application of neural networks for system identification of an adsorption column, *Neural. Comput. Appl.* **1** (1993) 160–165, doi: <https://doi.org/10.1007/BF01414435>.
37. K. V. *Kumar*, M. M. *de Castro*, M. *Martinez-Escandell*, M. *Molina-Sabio*, F. *Rodriguez-Reinoso*, Neural network and principal component analysis for modeling of hydrogen adsorption isotherms on KOH activated pitch-based carbons containing different heteroatoms, *Chem. Eng. J.* **159** (2010) 272–279, doi: <https://doi.org/10.1016/j.cej.2010.01.059>.
38. C. *Cojocar*, M. *Macoveanu*, I. *Cretescu*, Peat-based sorbents for the removal of oil spills from water surface: Application of artificial neural network modeling, *Colloids. Surf. A. Physicochem. Eng. Asp.* **384** (2011) 675–684, doi: <https://doi.org/10.1016/j.colsurfa.2011.05.036>.
39. R. M. *Aghav*, S. *Kumar*, S. N. *Mukherjee*, Artificial neural network modeling in competitive adsorption of phenol and resorcinol from water environment using some carbonaceous adsorbents, *J. Hazard. Mater.* **188** (2011) 67–77, <https://doi.org/10.1016/j.jhazmat.2011.01.067>.
40. M. *Molashahi*, H. *Hashemipour*, Experimental study and artificial neural network simulation of methane adsorption on activated carbon, *Korean. J. Chem. Eng.* **29** (2012) 601–605, doi: <https://doi.org/10.1007/s11814-011-0215-1>.
41. J. P. S. *Aniceto*, D. L. A. *Fernandes*, C. M. *Silva*, Modeling ion exchange equilibrium of ternary systems using neural networks, *Desalination* **309** (2013) 267–274, doi: <https://doi.org/10.1016/j.desal.2012.10.024>.
42. M. T. *Hagan*, H. B. *Demuth*, M. H. *Beale*, *Neural Network Design*, Pws Publ., Boston, 1996.
43. D. Z. *Antanasijević*, M. Đ. *Ristić*, A. A. *Perić-Grujić*, V. V. *Pocajt*, Forecasting GHG emissions using an optimized artificial neural network model based on correlation and principal component analysis, *Int. J. Greenhouse. Gas. Control.* **20** (2014) 244–253, doi: <https://doi.org/10.1016/j.ijggc.2013.11.011>.
44. L. *Khaouane*, O. *Benkortbi*, S. *Hanini*, C. *Si-Moussa*, Modeling of an industrial process of pleuromutilin fermentation using feed forward neural networks, *Braz. J. Chem. Eng.* **30** (1) (2013) 105–116, doi: <https://doi.org/10.1590/S0104-66322013000100012>.
45. D. S. *Lee*, J. M. *Park*, Neural network modeling for on-line estimation of nutrient dynamics in a sequentially-operated batch reactor, *J. Biotechnol.* **75** (1999) 229–239, doi: [https://doi.org/10.1016/S0168-1656\(99\)00171-6](https://doi.org/10.1016/S0168-1656(99)00171-6).
46. R. G. *Silva*, A. J. G. *Cruz*, C. O. *Hokka*, R. L. C. *Giordano*, R. C. *Giordano*, A hybrid feedforward neural network model for the cephalosporin C production process, *Braz. J. Chem. Eng.* **17** (2000) 587–598, doi: <https://doi.org/10.1590/S0104-66322000000400023>.
47. M. R. *Fagundes-Klen*, P. *Ferri*, T. D. *Martins*, C. R. G. *Tavares*, E. A. *Silva*, Equilibrium study of the binary mixture of cadmium–zinc ions biosorption by the *Sargassum filipendula* species using adsorption isotherms models and neural network, *Biochem. Eng. J.* **34** (2007) 136–146, doi: <https://doi.org/10.1016/j.bej.2006.11.023>.
48. R. C. *Deo*, M. *Şahin*, Application of the artificial neural network model for prediction of monthly standardized precipitation and evapotranspiration index using hydrometeorological parameters and climate indices in eastern Australia, *Atmospheric. Res.* **161-162** (2015) 65–81, doi: <https://doi.org/10.1016/j.atmosres.2015.03.018>.
49. Y. *Ammi*, L. *Khaouane*, S. *Hanini*, Prediction of the rejection of organic compounds (neutral and ionic) by nanofiltration and reverse osmosis membranes using neural networks, *Korean J. Chem. Eng.* **32** (2015) 2300–2310, doi: <https://doi.org/10.1007/s11814-015-0086-y>.
50. C. *Si-Moussa*, S. *Hanini*, R. *Derriche*, M. *Bouhedda*, A. *Bouzidi*, Prediction of high-pressure vapor liquid equilibrium of six binary systems, carbon dioxide with six esters, using an artificial neural network model, *Braz. J. Chem. Eng.* **25** (2008) 183–199, doi: <https://doi.org/10.1590/S0104-66322008000100019>.
51. M. *Carsky*, D. D. *Do*, Neural network modeling of adsorption of binary vapour mixtures, *Adsorption.* **5** (1999) 183–192, doi: <https://doi.org/10.1023/A:1008977528474>.
52. V. D. *Nguyen*, R. R. *Tan*, Y. *Brondial*, T. *Fuchino*, Prediction of vapor–liquid equilibrium data for ternary systems using artificial neural networks, *Fluid. Phase. Equilib.* **254** (2007) 188–197, doi: <https://doi.org/10.1016/j.fluid.2007.03.014>.
53. J. E. *Schmitz*, R. J. *Zemp*, M. J. *Mendes*, Artificial neural networks for the solution of the phase stability problem, *Fluid Phase Equilib.* **245** (2006) 83–87, doi: <https://doi.org/10.1016/j.fluid.2006.02.013>.
54. F. *Dreisbach*, R. *Staudt*, J. U. *Keller*, High pressure adsorption data of methane, nitrogen, carbon dioxide and their binary and ternary mixtures on activated carbon, *Adsorption.* **5** (1999) 215–227, doi: <https://doi.org/10.1023/A:1008914703884>.
55. M. *Sudibandriyo*, Z. *Pan*, J. E. *Fitzgerald*, R. L. *Robinson*, K. A. M. *Gasem*, Adsorption of methane, nitrogen, carbon dioxide, and their binary mixtures on dry activated carbon at 318.2 K and pressures up to 13.6 MPa, *Langmuir.* **19** (2003) 5323–5331, doi: <https://doi.org/10.1021/la020976k>.
56. B. *Rios*, F. M. *Stragliotto*, H. R. *Peixoto*, A. E. B. *Torres*, M. *Bastos-Neto*, D. C. S. *Azevedo*, C. L. *Cavalcante Jr*, Studies on the adsorption behavior of CO₂–CH₄ mixtures using activated carbon, *Braz. J. Chem. Eng.* **30** (2013) 939–951, doi: <https://doi.org/10.1590/S0104-66322013000400024>.
57. A. *Awadallah-F*, S. A. *Al-Muhtaseb*, Carbon dioxide sequestration and methane removal from exhaust gases using resorcinol–formaldehyde activated carbon xerogel, *Adsorption.* **19** (2013) 967–977, doi: <https://doi.org/10.1007/s10450-013-9508-5>.
58. Z. *Zhang*, M. *Xu*, H. *Wang*, Z. *Li*, Enhancement of CO₂ adsorption on high surface area activated carbon modified by N₂, H₂ and ammonia, *Chem. Eng. J.* **160** (2010) 571–577, doi: <https://doi.org/10.1016/j.cej.2010.03.070>.
59. P. *Ning*, F. *Li*, H. *Yi*, X. *Tang*, J. *Peng*, Y. *Li*, D. *He*, H. *Deng*, Adsorption equilibrium of methane and carbon dioxide on microwave-activated carbon, *Sep. Purif. Technol.* **98** (2012) 321–326, doi: <https://doi.org/10.1016/j.seppur.2012.07.001>.
60. Y. *Ben Torkia*, M. *Ben Yahia*, M. *Khalfaoui*, S. A. *Al-Muhtaseb*, A. *Ben Lamine*, Energetic investigation of the adsorption process of CH₄, C₂H₆ and N₂ on activated carbon: Numerical and statistical physics treatment, *Physica. B. Condens. Matter.* **433** (2014) 55–61, doi: <https://doi.org/10.1016/j.physb.2013.09.057>.
61. R. V. D. *Vaart*, C. *Huiskes*, H. *Bosch*, T. *Reith*, Single and mixed gas adsorption equilibria of carbon dioxide/methane on activated carbon, *Adsorption.* **6** (2000) 311–323, doi: <https://doi.org/10.1023/A:1026560915422>.
62. D. *Pino*, F. *Plantier*, D. *Bessieres*, Experimental determination of the adsorption isotherms in gas mixtures under extended pressure and temperature range, *J. Therm. Anal. Calorim.* **117** (2014) 1469–1477, doi: <https://doi.org/10.1007/s10973-014-3931-z>.
63. M. S. *Balathanigaimani*, H.-C. *Kang*, W.-G. *Shim*, C. *Kim*, J.-W. *Lee*, H. *Moon*, Preparation of powdered activated carbon from rice husk and its methane adsorption properties, *Korean J. Chem. Eng.* **23** (2006) 663–668, doi: <https://doi.org/10.1007/s11814-015-0086-y>.

- org/10.1007/BF02706811.
64. F. Ahmed, H. J. Cho, J. K. Kim, N. U. Seong, Y. K. Yeo, A real-time model based on least squares support vector machines and output bias update for the prediction of NO_x emission from coal-fired power plant, Korean. J. Chem. Eng. **32** (2015) 1029–1036, doi: <https://doi.org/10.1007/s11814-014-0301-2>.
 65. L. Khaouane, Etude et modélisation de la biosynthèse des antibiotiques à partir de différentes souches productrices – cas de pleuromutiline, PhD thesis, Université de Médéa, Algeria, 2013.
 66. E. M. E. -M. Shokir, E. S. Al-Homadhi, O. Al-Mahdy, A. A.-H. El-Midany, Development of artificial neural network models for supercritical fluid solvency in presence of co-solvents, Korean. J. Chem. Eng. **31** (2014) 1496–1504, doi: <https://doi.org/10.1007/s11814-014-0065-8>.
 67. H. Adib, S. Hassanajili, M. R. Sheikh-Kouhsar, A. Salahi, T. Mohammadi, Experimental and computational investigation of polyacrylonitrile ultrafiltration membrane for industrial oily wastewater treatment, Korean. J. Chem. Eng. **32** (2015) 159–167, doi: <https://doi.org/10.1007/s11814-014-0218-9>.

SAŽETAK

Modeliranje adsorpcije metana, dušika, ugljikova dioksida te njihovih binarnih i ternarnih smjesa na aktivnim ugljenima pomoću umjetne neuronske mreže

Hadjer Barki, Latifa Khaouane i Salah Hanini*

U ovom radu ispitana je primjena neuronskih mreža u modeliranju procesa adsorpcije smjese plinova (CO₂, CH₄ i N₂) na različitim aktivnim ugljenima. Izrađeno je sedam modela neuronskih mreža, karakteriziranih različitim strukturama s ciljem predviđanja adsorpcije smjesa plinova. Za testiranje neuronskih mreža primijenjen je skup od 417, 625, 143, 87, 64, 64 i 40 podatkovnih točaka za NN1 do NN7. Od ukupnih podataka 60 %, 20 % i 20 % rabljeno je za obuku, validaciju i testiranje sedam modela. Rezultati pokazuju dobar odnos predviđenih i eksperimentalnih vrijednosti za svaki model; pronađene su dobre korelacije ($R = 0,99656$ za NN1, $R = 0,99284$ za NN2, $R = 0,99388$ za NN3, $R = 0,99639$ za Q₁ za NN4, $R = 0,99472$ za Q₂ za NN4, $R = 0,99716$ za Q₁ za NN5, $R = 0,99972$ za Q₃ za NN5, $R = 0,99746$ za Q₂ za NN6, $R = 0,99783$ za Q₃ za NN6, $R = 0,9946$ za Q₁ za NN7, $R = 0,99089$ za Q₂ za NN7 i $R = 0,9947$ za Q₃ za NN7). Dodatno, usporedba predviđenih rezultata i klasičnih modela (Gibbsov model, generalizirani Langmuirov model i teorija idealne adsorpcije otopine) pokazuje da su modeli neuronskih mreža dali daleko bolje rezultate.

Ključne riječi

Aktivni ugljen, adsorpcija, smjesa plinova, modeliranje, neuronske mreže

Laboratory of Biomaterial and Transport Phenomena (LBMPT), University of Médéa, Alžir

*Izvorni znanstveni rad
Prispjelo 18. siječnja 2019.
Prihvaćeno 8. ožujka 2019.*